PERGAMON

International Journal of Multiphase Flow 25 (1999) 321–347

International Journal of Multiphase Flow

Effects of entrainment and deposition mechanisms on annular dispersed two-phase flow in a converging nozzle

S. Ho Kee King*, G. Piar

Laboratoire d'Energétique et de Thermique Industrielle de l'Est Francilien (LETIEF), Université Paris XII-Val de Marne, IUT de Créteil, Avenue du Général de Gaulle, 94010, Créteil Cédex, France

Abstract

This paper is intended to establish a simple three-field model, which gives good agreement with a converging nozzle data previously obtained. The problems encountered in developing a mathematical model for two-phase flow are numerous and generally complex. More particularly, the main difficulties concern the closure relations generally correlated empirically and which govern the various transfers at the interfaces and walls. Our methodology consists in taking into account at first the limits of the annular dispersed configuration before reaching step by step its complete description. Such a procedure underlines the necessity to describe the entrainment and deposition mechanisms in order to get a better annular dispersed two-phase flow understanding. © 1999 Elsevier Science Ltd. All rights reserved.

Keywords: Two-phase flow; Air-water; Annular dispersed flow; Converging nozzle; One-dimensional model; Closure laws; Entrainment rate; Deposition rate; Entrained liquid fraction; Onset of entrainment

1. Introduction

The study of two-phase flows is necessary to evaluate or optimize the performances of many industrials systems currently encountered in chemical, thermal or nuclear engineering. For example, in petroleum industry, where fluids are generally in pressurized tanks storage, the security of industrial equipment relies on the correct sizing of the safety valve to prevent for an eventual accidental rupture of a liquefied tank, or the protection of chemical reactors against thermal runaway.

* Corresponding author. Tel.: (33) (1) 45 17 18 41; Fax: (33) (1) 45 17 18 42; E-Mail: hokee@univ-paris12.fr

PII: S0301-9322(98)00043-3

The purpose of this paper is to investigate how such a flow develops through a converging nozzle. Owing to the present state of knowledge, we are only interested in developing one-dimensional (1D) flow models.

Droplet moisture exchange is an important factor for mass transfer of annular dispersed two-phase flows. Such a flow is characterized by a central gas core containing droplets flowing with a velocity more rapid than the liquid film on the pipe wall. Its complete modeling is based on writing the conservation equations of mass, momentum and energy for each one of the three-fields : liquid film, gas and dispersed droplets.

The problems generally encountered in modeling two-phase flows are in establishing analytically the transfers between the fluids under consideration and the walls, on the one hand, and between the fluids themselves at the interfaces on the other hand. The laws giving these various transfers allow one to close the conservation equations system and are so called closure laws. Among these laws, the more difficult to specify are the deposition and entrainment rates not yet as well-known as, for example, film-gas, gas-droplets interfacial friction, or wall friction.

Our work is essentially based on air–water experiments performed at CEA/Grenoble by Lemonnier and Camelo (1993) and Selmer Olsen (1991) on the *FOSSEGRIMEN* flow loop, with an annular liquid injection mode. This loop is designed by Selmer Olsen in order to produce annular dispersed critical air–water two-phase flow. The experimental data are collected from a vertical downward converging nozzle with a 10 mm diameter long throat : data of pressure and film thickness profiles, maximum gas mass flowrate, size and velocity of droplets at the nozzle exit. The experimental setup and the techniques of measure are described in detail by Selmer Olsen (1991) and Lemonnier and Camelo (1993).

In a first step, two simplified flow models are utilized to analyze the experimental data : totally dispersed flow and purely annular flow models. It appears clearly that neither the liquid film or dispersed droplets can be neglected in Lemonnier and Selmer Olsen's experiments. However, it must be emphasized that when the gas mass quality is very high the flow is basically dispersed; so the two-field model predicts quite well the maximum gas mass flowrate and exit liquid droplet velocities (Lemonnier and Camelo 1993; Ho-Kee-King 1996). Therefore, the three-field model must verify numerical results identical to those of the two-field model when the two-phase flow tends to become essentially dispersed.

At the beginning, the experiments of Lemonnier and Selmer Olsen have been carried out to characterize the effects of non-equilibrium. These authors have already compared their data with predictions of a dispersed flow model (*DFM*), which neglects the effect of liquid film presence at walls, and where only the difference of velocities between the phases is taken into account. With the two-field model presented here, which assumes the two-phase flow being totally dispersed, any kind of non-equilibrium (mechanical or thermal) is taken into account. In the considered experiments, predictions of such a model have confirmed that the main source of non-equilibrium is effectively the mechanical's one and that thermal non-equilibrium between the phases can be neglected.

The next step consists in a more complete modeling with the "frozen" three-field model, the whole effects of droplet entrainment and deposition being neglected. So, for the model closure, the main assumption, which is highly speculative, is that a quasi-equilibrium is established between the annular film, at walls and the dispersed gas core from the nozzle inlet. The

purpose of such a step in our work is to highlight the effects on pressure profile of the entrained liquid fraction at the nozzle inlet, more particularly at the throat inlet. In the presented experiments, comparisons of data with predictions of pressure and film thickness profiles, showed that droplet moisture exchange between the liquid film and the dispersed central gas core would take place in a large majority in the converging part of the nozzle. After this step, we have intended to give a more detailed description of annular dispersed air–water flows in nozzles with the three-field model, incorporating entrainment and deposition mechanisms.

For lack of suitable correlations of entrainment and deposition rates in literature, our objective is to search for a deposition–entrainment model which provides a good agreement between the three-field model's predictions, with available experimental data obtained in a converging nozzle.

2. Limits configurations of annular dispersed two-phase flow modeling

The two flow models presented in this section are the totally dispersed flow model (*two-field model*), where the presence of liquid film is neglected, on the one hand, and the purely annular flow model (*PAFM*), assuming negligible the effects of dispersed droplets in the gas core, on the other hand.

The thermodynamical properties of the fluids are defined by assuming that air follows perfect gas laws and water to be an incompressible fluid.

2.1. Totally dispersed flow model (two-field model)

Ho-Kee-King (1996) has presented a 7-equation dispersed flow model, namely the *two-field model*, based on six independent balance equations (one mass balance, one momentum balance and one energy balance for each of the two phases), and one equation which imposes the pipe's profile (see the Appendix). This last equation appears explicitly in the system because of the following selected independent variables:

$$\dot{M}_G, \dot{M}_L, u_G, u_L, H_G, H_L, P, \tag{1}$$

where $\dot{M}_G$ is the gas mass flowrate (kg/s), $\dot{M}_L$ the dispersed liquid mass flowrate (kg/s), u_G the averaged gas velocity (m/s), u_L the averaged dispersed droplets velocity (m/s), H_G the averaged mass enthalpy (J/kg), H_L the averaged droplets mass enthalpy (J/kg), and P the mixture pressure (N/m^2).

This model differs from the 5-equation dispersed flow model (DFM) proposed by Lemonnier and Selmer Olsen (1992), only by the fact that it includes the differences of temperatures between the phases in addition to the mechanical non-equilibrium.

The four closure relations to be provided to the two-field model are the wall friction from the gas phase τ_{Gp} (N/m^2), the interfacial friction between gas and droplets τ_{GL} (N/m^2), the droplets diameter d (m) and the heat flux at gas-droplet interfaces $\dot{Q}_{LG}$ (J/s.m^2). For the first three relations just mentioned, we have utilized those of DFM.

The wall friction is given by the classical Blasius's relation for a single fluid flow in pipe:

$$\tau_{\mathrm{Gp}} = \frac{1}{2} f \rho u^2; f = 0.0791 Re_{\mathrm{G}}^{-0.25},\ Re_{\mathrm{G}} = \frac{\rho_{\mathrm{G}} u_{\mathrm{G}} D}{\mu_{\mathrm{G}}}, \tag{2}$$

where ρ and u are the density (kg/m^3) and the velocity (m/s) of two-phase mixture, respectively, D the pipe diameter (m) and μ_{G} the gas dynamic viscosity (kg/m.s).

The interfacial friction at gas-droplets interfaces proposed by Selmer Olsen is correlated as:

$$\tau_{\mathrm{GL}} = \frac{1}{2} C_{\mathrm{D}} \rho_{\mathrm{G}} (u_{\mathrm{G}} - u_{\mathrm{L}}) |u_{\mathrm{G}} - u_{\mathrm{L}}|; C_{\mathrm{D}} = 6.3 Re_d^{-0.385},\ Re_{\mathrm{d}} = \frac{\rho_{\mathrm{G}} d |u_{\mathrm{G}} - u_{\mathrm{L}}|}{\mu_{\mathrm{G}}}. \tag{3}$$

The droplet size is calculated from the maximum stable diameter according to Berne (1983):

$$d = \frac{25}{42} \left(\frac{1}{\pi^2} \frac{24}{2 + 3\rho_{\mathrm{L}}/\rho_{\mathrm{G}}} \right)^{3/5} \left(\frac{\sigma}{\rho_{\mathrm{L}}} \right)^{3/5} \left(\frac{u_*^3}{\kappa R} \right)^{-2/5} \tag{4}$$

which depends of the friction velocity u_* defined as:

$$u_* = \sqrt{\tau_{\mathrm{Gp}}/\rho}, \tag{5}$$

where κ is the Von Kármán constant ($\approx$0.41), R the pipe radius (m), ρ_{L} the liquid density, and σ the liquid surface tension (N/m).

For the last closure relation, the heat flux from the liquid dispersed phase to the gas phase is correlated by (Richter, 1983; Dobran, 1987):

$$\dot{Q}_{\mathrm{LG}} = \tilde{h}_{\mathrm{L}} (T_{\mathrm{L}} - T_{\mathrm{G}}), \tag{6}$$

where T_{L} and T_{G} are the averaged temperature of the droplets and the gas, respectively (K), and the heat flux coefficient $\tilde{h}_{\mathrm{L}}$ is given by analogy with a flow surrounding a single sphere (Bird et al., 1960):

$$Nu_{\mathrm{L}} = \frac{\tilde{h}_{\mathrm{L}} d}{\lambda_{\mathrm{G}}} = 2 + 0.6 Re_d^{1/2} Pr_{\mathrm{G}}^{1/3}, \tag{7}$$

where λ_{G} is the gas heat conductivity (W/K.m).

Figure 1 presents comparisons of predictions with data of maximum gas mass flowrate, droplet velocity, and size at the nozzle exit, for all the experiments performed by Lemonnier and Camelo (1993) when the upstream pressure is set to 2 bar and varying liquid mass flowrate. The gas mass quality is ranged between 96 and 25%.

We first compared predictions of the two-field model proposed here (Fig. 1, starry symbol) with still those of the two-field model, but setting a heat flux coefficient sufficiently high so as to reach for an effective heat transfer between the two phases (Fig. 1, squared symbol). These last predictions are obviously identical to DFM's ones.

Such a comparison showed equivalent results, so Selmer Olsen's assumption in the DFM is confirmed : the effects of the thermal non-equilibrium can be neglected for these experiments. It should be noticed that for a liquid mass flowrate below 50 kg/h the calculated maximum gas mass flowrate is slightly higher when the thermal equilibrium is not imposed.

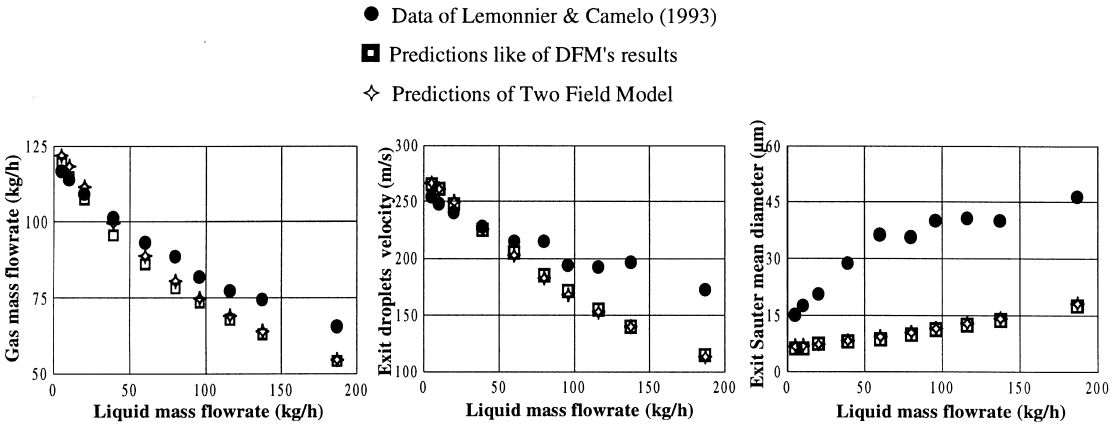

Fig. 1. Comparison of data (circular symbol) with (a) predictions of two-field model (starry symbol) and (b) predictions of two-field model but imposing thermal equilibrium between the phases (squared symbol). The upstream pressure is constant and equal to 2 bar.

Next, a comparison of predictions (Fig. 1, starry or squared symbol) with data (Fig. 1, circular symbol) showed, according to the conclusions of Lemonnier and Camelo (1993), that:

- with a liquid mass flowrate value less than 50 kg/h, the maximum gas mass flowrate and exit droplet velocity are well predicted;
- for higher liquid mass flowrates, the discrepancies increase with the increase of the liquid mass flowrate;
- the droplet size predicted at the nozzle exit is always smaller than the measured drop size, the differences become more significant with the increase of the liquid mass flowrate. This could be the consequence of a phenomena of drops coalescence occurring from the nozzle outlet and the location where the measurements had been performed (at 15 mm apart from the throat end, Lemonnier and Camelo 1995).

If now we look at the case where the gas quality is equal to 25%, or the liquid mass flowrate is equal to 187.6 kg/h (see Fig. 1), we have also compared the measured pressure profile (Fig. 2, symbol) with the pressure profiles predicted by the two-field model.

The first pressure profile (Fig. 2, thin full line) is obtained with the predicted critical gas mass flowrate, which is calculated iteratively so that the downstream pressure becomes equal to 1 bar: its value of 55.2 kg/h is lower than the experimental value (equal to 65.8 kg/h). Thus, it is remarked that, although the downstream pressure is the atmospheric pressure, the calculated pressure drop inside the throat disagrees with the data.

The second pressure profile (Fig. 2, intermittent line) is calculated with the measured gas mass flowrate (equal to 65.8 kg/h). It can be noticed that, up to a certain section, a good agreement is reached with the data and, downstream, the pressure drops so fast that the predictions present a vertical tangent. If we refer to the detailed analysis of Bilicki et al. (1987) on the topological description of the ensemble of solutions, the point offering a vertical tangent

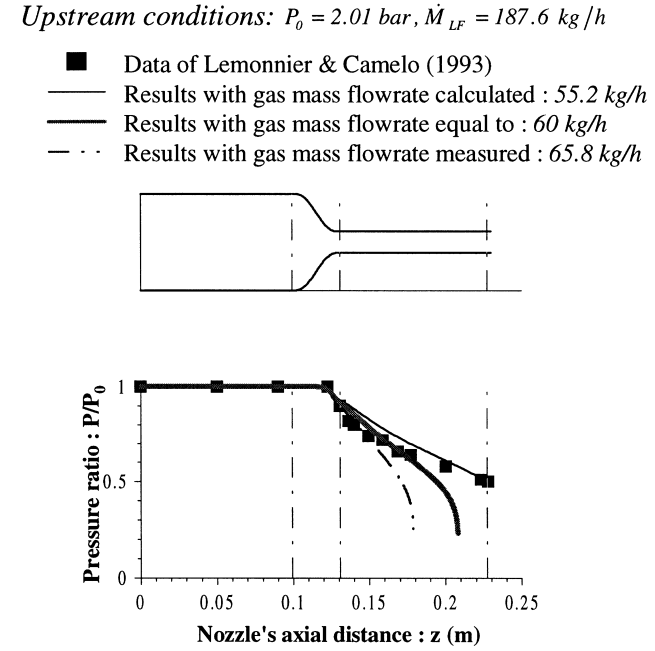

Fig. 2. Comparison with measured pressure (symbol) and predictions of two-field model for various gas mass flowrate values.

should be a turning point ; so the nature of the two-phase flow is critical and the flow is not feasible.

Figure 2 also presents another pressure profile obtained with an intermediate value of gas mass flowrate, and it illustrates the displacement of the critical section towards the throat exit.

The two-field model can reproduce successfully the experimental results only when the flow is basically dispersed (with high gas mass quality or low liquid mass flowrate). In the experiments at an upstream pressure of 2 bar presented in this section, the discrepancies appear significantly when the liquid flowrate is higher than 50 kg/h: the maximum gas mass flowrate and the exit droplet diameter and velocity are all underestimated, and the pressure drop inside the nozzle throat is not well reproduced. Moreover, since the presence of film liquid is neglected, the two-field model is not able to describe the effect of the annular gas–liquid configuration at the nozzle inlet.

The reasons evoked by Selmer Olsen (1991) and Lemonnier and Camelo (1993) in their analysis, are focused on the fact that the liquid film should play an important role on the acceleration of the gas–liquid flow. Then, this could explain the underestimations of the maximum gas flowrate and, in the same way, the influence of the gas mass flowrate on the pressure profile illustrated in Fig. 2.

In order to highlight the effects of the film on the mechanical non-equilibrium between the phases, we have analyzed the data with the other limit flow model's predictions, which assumes all the liquid phase as film on the nozzle walls.

2.2. Purely annular two-phase flow model (PAFM)

The liquid injection mode at the nozzle inlet is annular, and it is assumed here that the flow pattern remains the same along the nozzle. The assumptions of the previous flow model are preserved, except that the dispersed liquid phase is now neglected and the film thickness is assumed uniformly distributed all around the pipe wall. The system of the equations of PAFM are presented in the Appendix.

Concerning the closure laws, the parietal friction τ_{Fp} (N/m^2) is exerted from the liquid film and the interfacial friction τ_{GF} (N/m^2) at the interface between the surface of the liquid film and the gas core. The surface of the liquid film is assumed to be a rough "pseudo-wall" (Dobran, 1987; Nigmatulin, 1991). The closure relations are expressed as:

$$\text{If } Re_F < 1600,\ \tau_{Fp} = \frac{2u_F}{\delta} \quad \text{and} \quad \tau_{GF} = \tau_{Fp}.$$

$$\text{If } Re_F \geq 1600,\ \tau_{Fp} = \frac{1}{2} C_w \rho_F u_F^2,\ C_w = 0.083 Re_F^{-0.25},\ u_{FG} = 8/7 u_F.$$

$$\tau_{GF} = \frac{1}{2} C_{GF} \rho_G (u_G - u_{FG})^2,\ C_{GF} = 0.0791 Re_G^{-0.25} \left[1 + 24(1 - \sqrt{\alpha_G}) \left(\frac{\rho_F}{\rho_G} \right)^{1/3} \right] \tag{8}$$

where δ is the mean averaged thickness (m), ρ_F the liquid film density (kg/m^3), u_F the averaged liquid film velocity (m/s), u_{FG} the velocity at the interface between the liquid film and the gas core (m/s), α_G the averaged gas fraction and Re_F the film Reynolds number defined as:

$$Re_F = \frac{4\rho_F u_F \delta}{\mu_F} \tag{9}$$

The heat flux $\dot{Q}_{FG}$ exerted from the liquid film to the gas core is correlated from:

$$\dot{Q}_{FG} = \tilde{h}_F (T_F - T_G), \tag{10}$$

where T_F is the averaged film temperature (K), and the heat flux coefficient is given by analogy with Colburn's relation:

$$Nu_F = \frac{\tilde{h}_F D \sqrt{\alpha_G}}{\lambda_G} = 0.023 Re_G^{0.8} Pr_G^{0.4}. \tag{11}$$

Figure 3 compares, for the same experimental conditions in Fig. 2, the measured pressure profile to PAFM's predictions.

The pressure profile which is calculated with the measured gas mass flowrate (Fig. 3, full line) is obviously beyond the data of pressure.

To get closer to the measured pressure profile, a very great value of gas mass flowrate should be introduced, as shown the pressure profile predicted with a higher gas mass flowrate equal to 95 kg/h (Fig. 3, intermittent line), whereas the measured value is 65.8 kg/h.

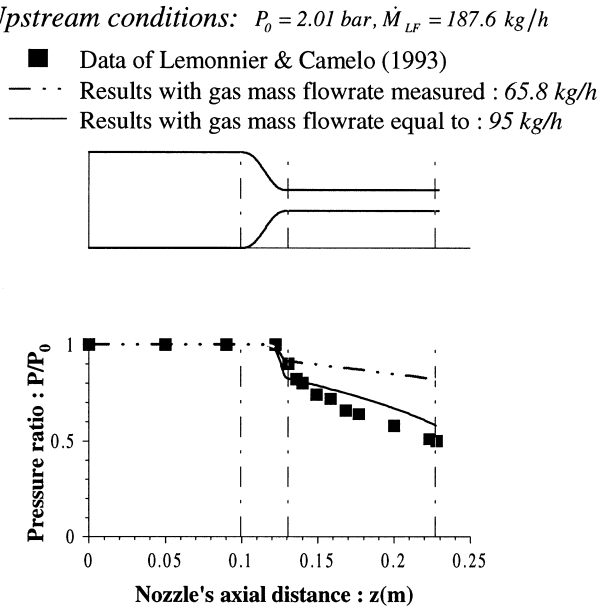

Fig. 3. Comparison with measured pressure (symbol) and predictions of PAFM for various gas mass flow-rate values.

The PAFM is also unable, as the two-field model, to predict well the experimental results, but it appears clear that the liquid film is a source of high mechanical non-equilibrium, as underlined by Lemonnier and Camelo (1993). The influence of gas mass flowrate on the pressure profile, illustrated in Fig. 3, gives us the idea that the improvement of the predicted maximum gas mass flowrate in Fig. 1 could be possible if we introduce the liquid film field into the flow modeling. In other words, a good description of the experiments presented here requires a complete modeling of the annular dispersed structure of the flow.

2.3. Conclusion

By considering the two extreme configurations of the annular dispersed flow pattern, the discrepancies between predictions and experimental results are obviously revealed relating to pressure profiles inside the throat, maximum gas mass flowrates, exit droplets velocities and diameters (Figs. 1–3).

For the first time, in conformity with the authors Selmer Olsen and Lemonnier, the two-field model has showed that, in all the experiments at an upstream pressure of 2 bar, the main non-equilibrium between the liquid and gas phases is of mechanical nature: the temperature of the liquid and gas phases does not differ significantly. With regard to the data, the discrepancies could be the result of there being no account for the liquid film flowing along the nozzle walls, as has been suggested by Selmer Olsen and Lemonnier.

The analysis of data with the PAFM allows us to illustrate the important role of the liquid film on the mechanical non-equilibrium between the phases, on the prediction of the maximum gas mass flowrate.

Then, again in agreement with Selmer Olsen and Lemonnier, it could be possible to bring improvements to the predictions with a more complete description of the annular dispersed structure.

Although it has been clear from the beginning that an annular dispersed flow model must be established to describe these experiments in a converging nozzle, this step leads us to the understanding of how an annular or dispersed configuration has a significant effect on the maximum gas flowrate, due to different types of momentum transfer between the gas phase and the liquid phase as film or droplets.

From here, we have started on the modeling of the annular dispersed flow. Our purpose is to develop a three-field model, which not only accounts for frictions and heat flux already introduced in the two-field model and the PAFM, but also for the mass transfer between the liquid film and the gas core. Selmer Olsen (1991) has shown the necessity to introduce the liquid deposition and entrainment mechanisms in order to take into account the non-stabilization of the two-phase flow in the nozzle.

The main difficulty in the complete modeling of annular dispersed two-phase flow, is the increase of the number of closure relations. Consequently, we have intended to reach it step by step by assuming for a start, in the next section, that all the effects due to entrainment and deposition processes are negligible.

3. "Frozen" Three-Field Model

Our primary approach to the annular dispersed two-phase flow model is to assume negligible the liquid mass transfer, in the mass balance equations as well as in the momentum and energy balance equations.

The whole correlations required for the closure model have been defined in the previous sections, and the assumptions of the two flow models have also been retained.

A distribution of the total liquid mass flowrate between the film and the droplets is set upstream of the nozzle. Introducing the measured value of the gas mass flowrate, pressure profiles are calculated with varying film mass flowrate or entrained liquid (Figs. 4 and 5).

The entrained liquid fraction E is defined as the ratio between the liquid mass flowrate dragged along the gas core from the film surface, and the total liquid mass flowrate.

Under the same experimental conditions than in Figs. 2 and 3, Fig. 4 shows that:

- If we assume a rather annular gas–liquid configuration, with a high film mass flowrate (equal to 180 kg/h with respect to the total liquid mass flowrate of 187.6 kg/h), or a low entrained liquid fraction E of about 0.2, the predicted pressure profile is obviously beyond measured points of pressure (Fig. 4, intermittent line): these results are similar to those of PAFM (see Fig. 3).

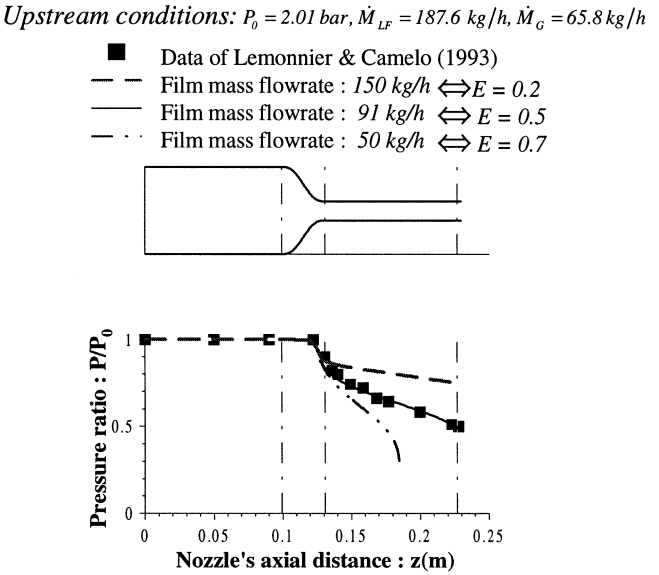

Fig. 4. Comparison with measured pressure (symbol) and predictions of "Frozen" three-field model for various entrained liquid fraction values.

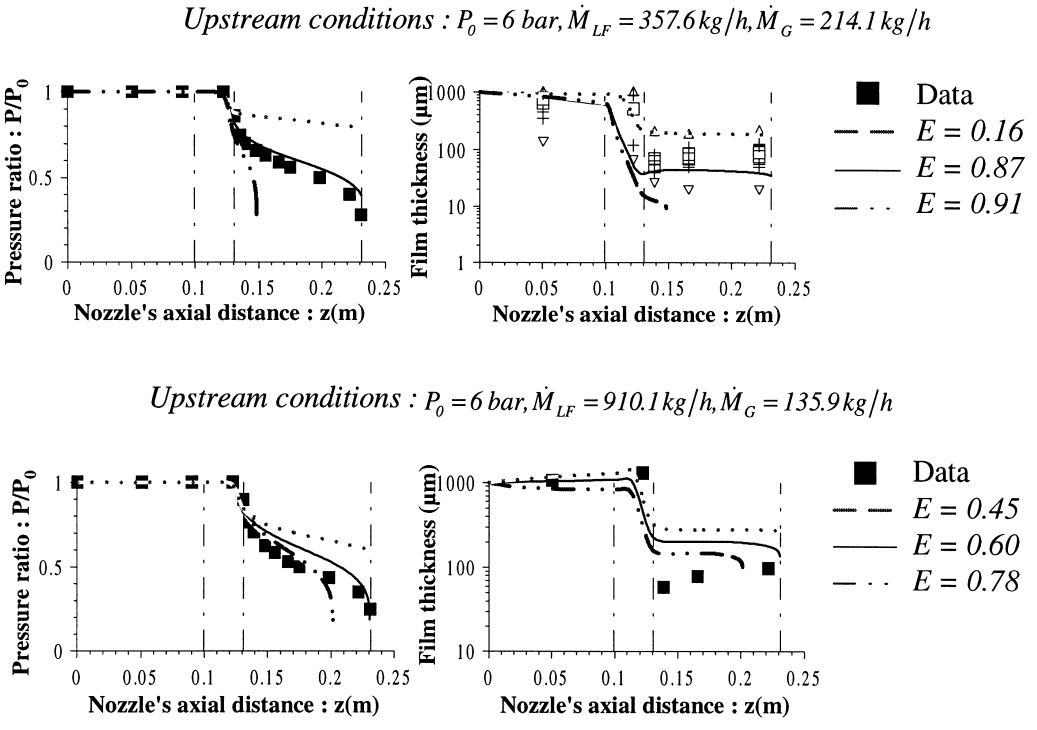

Fig. 5. Comparison of measured pressure and film thickness (symbols) with predictions of "Frozen" three-field model for various entrained liquid fraction values. The symbol (□) represents the mean film thickness, the crosses (+) indicate one standard deviation up or down, and the arrow tips (△ and ▽) indicate extreme values.

- If we assume a rather dispersed gas–liquid configuration, with an important amount of entrained liquid, the predicted pressure drop is far too considerable inside the throat (Fig. 4, mixed line): the results are now similar to those of the two-field model (see Fig. 2).
- However, with a certain value of entrained liquid (equal to 0.5), the pressure profile is well predicted (Fig. 4, full line).

Fig. 4 proves the existence of distribution film-droplets of the total liquid mass flowrate, with which the pressure profile gets close to the measured profile. In other words, the entrained liquid fraction at the nozzle inlet has a significant effect on the calculation of the pressure profile.

It is at the vicinity of the throat inlet that the influence of the entrained liquid fraction value is significant on the prediction of the pressure drop. As the upstream gas–liquid configuration is annular, a droplet moisture exchange between the liquid film and dispersed droplets can generate the appropriate distribution film-droplets at the neighborhood of the throat inlet.

In Fig. 5, the strong influence of the entrained liquid fraction E, is also observed for two other experimental conditions, as well as for the pressure profiles as on evolution of film thickness. It is noticed that an insufficient pressure drop inside the throat occurs for the case of the higher total liquid mass flowrate.

By assuming the gas mass flowrate to be equal to the measured one, we have analyzed the effects of the entrained liquid fraction at the inlet, on the pressure and film thickness profiles. The great sensitivity with respect to the value of the entrained liquid fraction, is located at the vicinity of the throat inlet. This suggests that an important liquid entrainment occurs along the converging part of the nozzle, since the liquid injection is annular. The growth of the data of film thickness shown in Fig. 5 suggests a liquid deposition along the nozzle throat.

The analysis of the data with the "Frozen" three-field model shows that the liquid mass transfer between the film and the gas core plays a non-negligible role on the evolution of the annular two-phase flow through the converging nozzle. Furthermore, combined with the experimental results, it allows a rough localization of the entrainment and deposition phenomena in the nozzle.

From the previous results, we can now go to the next step, which is to investigate the correlations of entrainment and deposition rates in order to complete the three-field model presented in the Appendix. This model is a 10-equation, annular dispersed, two-phase flow model, which also accounts for mechanical non-equilibrium as well as thermal non-equilibrium, and liquid mass exchange between the film and the gas core by droplet deposition and entrainment (see the Appendix).

4. With liquid mass exchange correlations from literature

In the three-field model, the rates of entrainment and deposition, $\dot{m}_E$ and $\dot{m}_D$ (kg/s.m^2), respectively, are present in each of the balance equations established for liquid film and dispersed droplets. In addition to closure relations specified for the "frozen" three-field model, it remains to define the relations of deposition and entrainment rates.

Table 1
Three major categories of existing correlations of mass transfer by entrainment and deposition, expressed from independent flow variables

- Hutchinson and Whalley (1973) and Whalley and Hewitt (1978):

$$\begin{cases} \dot{m}_D = kC \\ \dot{m}_E = kC_\infty \end{cases}; k = 87u_* \sqrt{\frac{\mu_L^2}{D\sigma\rho_L}}, u_* = \sqrt{\frac{\tau_{GF}}{\rho_G}}, C = \rho_L \frac{\alpha_L}{\alpha_L + \alpha_G},$$

where equilibrium droplets concentration C_∞ depends on $\tau_i\delta/\sigma$

- Hewitt and Govan (1990):

$$\dot{m}_D = kC; k\sqrt{\frac{\rho_G D}{\sigma}} = \begin{cases} 0.18 & \text{if } C/\rho_G < 0.3 \\ 0.083(C/\rho_G)^{-0.65} & \text{if } C/\rho_G > 0.3, \end{cases}$$

$$\dot{m}_E = 5.75 \times 10^{-5} \dot{M}_G \left[(\dot{M}_F - \dot{M}_F^*)^2 \frac{D\rho_L}{\sigma\rho_G^2} \right]^{0.316} \quad \text{if } \dot{M}_F > \dot{M}_F^*,$$

$$\text{with } \frac{\dot{M}_F^* D}{A\mu_F} = Re_F^* = \exp\left(5.8504 + 0.4249 \frac{\mu_G}{\mu_F} \sqrt{\frac{\rho_F}{\rho_G}} \right).$$

- Nigmatulin (1991):

$$\dot{m}_D = \frac{4\dot{M}_L}{\pi D D_h} 0.3(1 - 7.5\alpha_L) \frac{d^2\rho_F}{18\mu_G} \frac{\tau_{GF}}{\rho_G D_h u_G},$$

$$\dot{m}_E = \dot{m}_E^{(c)} + \dot{m}_E^{(d)} \text{ with } \begin{cases} \dot{m}_E^{(c)} = k^{(c)} \dot{m}_D; \; k^{(c)} = 1 - 0.01\alpha_L^{-0.17} (\rho_G/\rho_L)^{0.67} \\ \dot{m}_E^{(d)} = \frac{4\dot{M}_F}{\pi^2 D D_h} 0.55 \left(\frac{\rho_L}{\rho_G} \right)^{0.5} \bar{\mu}^{(\sigma g)} Re_F^{-1} (We_{GF} - We_{GF}^*)^{0.85}. \end{cases}$$

From a review of existing correlations, three major categories of relations of mass transfer could be distinguished and are listed in Table 1. In each of these categories, the entrainment mechanism is due to the shearing-off of roll wave crest by streaming gas flow. Nigmatulin (1991) has assumed another mechanism, in addition to the preceding one, due to shocks produced by depositing droplets of the flow core striking the film, and referred to as a shock splash break-away, which is correlated as directly proportional to the droplet deposition rate.

Figure 6 illustrates the pressure and film mass flowrate profiles calculated from the three-field model, with each one of the correlations presented in Table 1, in different experimental conditions.

It had not be possible with the last two models suggested by Hewitt and Govan (1990) and Nigmatulin (1991), to describe the entrainment and the deposition along the converging nozzle: there's almost no variation of film mass flowrates (Fig. 6). Furthermore, it had been necessary, as in the "Frozen" three-field model, to fix from the channel inlet a film-droplet distribution of the total liquid mass flowrate, which is not compatible with the upstream experimental conditions.

Nevertheless, the first model of deposition–entrainment according to Whalley and Hewitt (1978) and Hutchinson and Whalley (1973), is the only one which has succeeded to express an important mass exchange between film and gas core in the converging part of the nozzle from a rather annular upstream liquid configuration, for all the considered experiments (Fig. 6). However, the predicted pressure drops more rapidly before the exit throat and the film flowrate goes on decreasing inside the throat: then the entrainment is occurring, whereas Selmer Olsen had noticed, experimentally, a liquid re-deposition on the film surface.

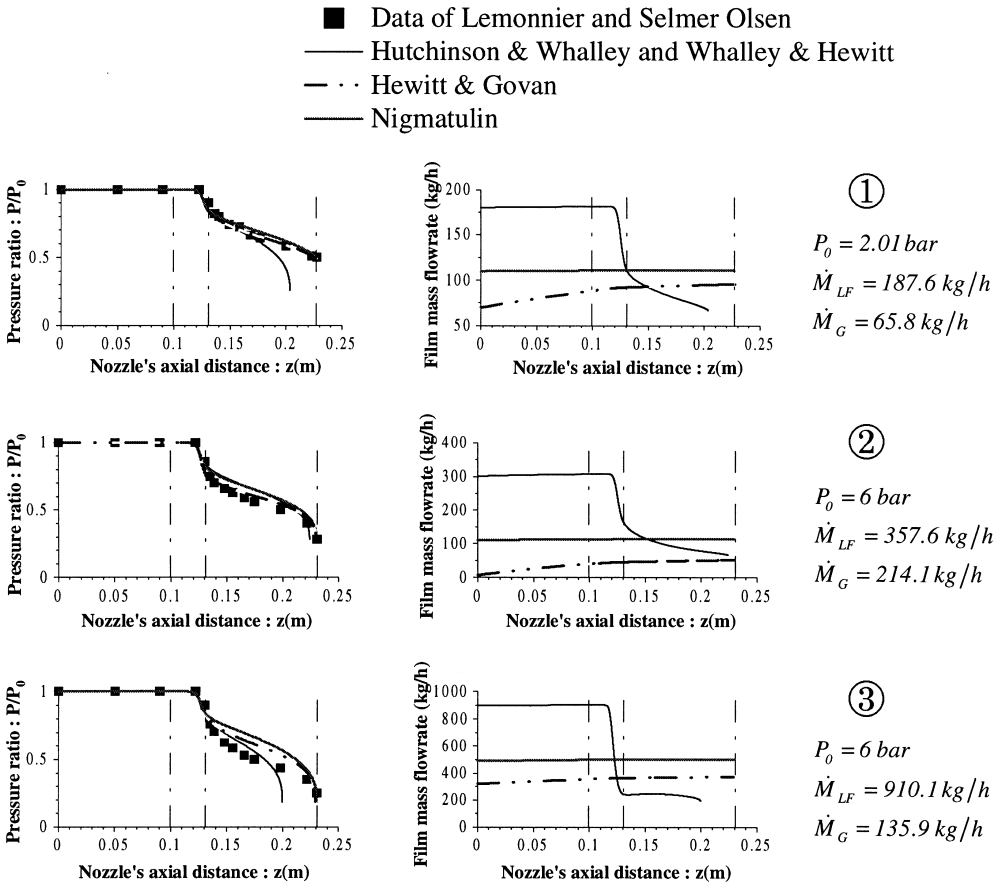

Fig. 6. Comparison of data with predictions of pressure and film mass flow-rate of the three-field model from mass transfer correlations according to different authors (Hutchinson and Whalley, 1973; Whalley and Hewitt, 1978; Hewitt and Govan, 1990; Nigmatulin, 1991), in experimental conditions performed in a converging nozzle.

It is clear that investigations are necessary to improve the predictions in a converging nozzle. The only correlations which can succeeded in describing the experiments of Lemonnier and Selmer Olsen, are those proposed by Hutchinson and Whalley (1973) and Whalley and Hewitt (1978) who, moreover, had agreed on the necessity to bring improvements to their relation of entrainment rate.

More recently, Nigmatulin et al. (1996) have modified their correlations of droplet deposition and entrainment rates using data from steam–water flows. It is conceivable to analyze the data in a converging nozzle with these relations, but from here, we have decided to focus on the simple model of entrainment rate proposed by Hutchinson and Whalley (1973). This is the subject of the next section, where other experimental data are used, which are more specific to the liquid mass exchange.

5. Investigating a simple model of entrainment rate

In view of a better understanding of entrainment and deposition mechanisms, we have applied the various mass transfer correlations listed in Table 1, to the experiments performed by Cousins et al. (1965). These authors had measured the entrained liquid fraction E from the film to the gas core, from annular air–water two-phase flow through a channel of constant cross section.

The investigations are based on three distinct experimental conditions performed at an upstream pressure equal to 2.76 bar, and varying film Reynolds numbers and gas mass flowrates.

The experiments of Cousins et al. (1965) had been described successfully with the correlation of entrained liquid fraction E, elaborated by Ishii and Mishima (1981). This one is expressed as following with an exponential relaxation function in the developing flow region, on the one hand, and with a constant E_∞ which depends on the entrance conditions in the fully developed region on the other hand:

$$E = \begin{cases} (1 - e^{-1.87.10^{-5}\zeta^2})E_\infty & \text{if } \zeta < 440 \\ E_\infty & \text{if } \zeta \geq 440, \end{cases} \tag{12}$$

where the equilibrium value of entrained fraction E_∞ is given by:

$$E_\infty = \tan h(7.25 \times 10^{-7} We^{1.25} Re_{\mathrm{LF}}^{0.25}) \tag{13}$$

and the dimensionless distance ζ by:

$$\zeta = \frac{z}{D_h} We^{-0.25} Re_{\mathrm{LF}}^{0.5}, \tag{14}$$

with Re_{LF} the total liquid Reynolds number, D_{h} the pipe hydraulic diameter, z the axial distance from pipe inlet, and We the entrainment Weber number defined by:

$$We = \frac{\rho_{\mathrm{G}} j_{\mathrm{G}}^2 D_{\mathrm{h}}}{\sigma} \left(\frac{\rho_{\mathrm{F}} - \rho_{\mathrm{G}}}{\rho_{\mathrm{G}}} \right)^{1/3}, \tag{15}$$

j_{G} is the gas superficial velocity.

The calculations of entrained fraction are illustrated in Fig. 7 (thin full line), showing that a good agreement with experimental data is achieved. Afterwards, these curves will be used as the basis of comparison with local relations of entrainment and deposition rates.

Kataoka and Ishii (1983) had also distinguished, in the experiments of Cousins et al. (1965) another region at the near-vicinity to the channel inlet, namely the geometry-dependent inlet region, where the droplets entrainment rate is almost non-existent.

As for Lemonnier and Selmer Olsen's experiments, the various mass transfer correlations of Table 1 have been introduced in the three-field model.

As for the results obtained in the previous section, the two last deposition–entrainment models proposed by Hewitt and Govan (1990) and Nigmatulin (1991) have not given satisfactory predictions: the differences with data are too large. It is, again the correlations of Whalley and Hewitt (1978) and Hutchinson and Whalley (1973) which allowed the predictions

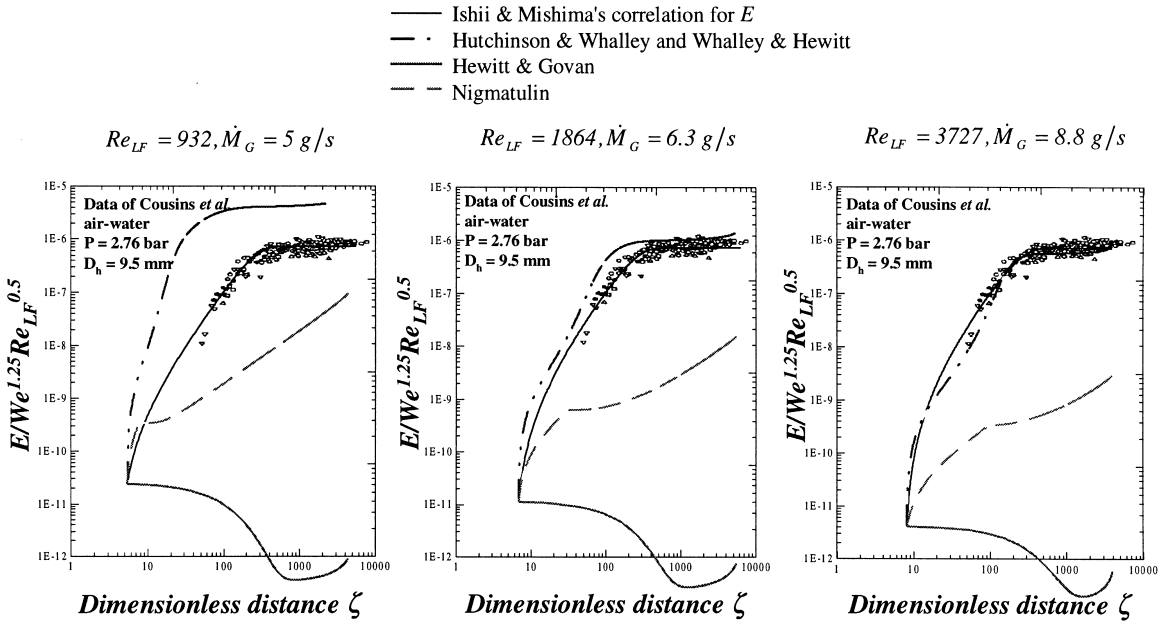

Fig. 7. Comparison of data of Cousins et al. (1965) with: (a) entrained fraction predicted from relation developed by Ishii and Mishima (1981); (b) predictions of three-field model obtained from various mass transfer correlations (see Table 1).

of E to get close to the data, the predictions-data differences being more significant for the case of lower film Reynolds number.

The conclusions are similar to those for Lemonnier and Selmer Olsen's experiments, strengthening thus our decision to investigate from the deposition and entrainment rate relations of Whalley and Hewitt and Hutchinson and Whalley. In accordance with the opinion of these authors, we have to bring modifications to the entrainment rate relation, with a view to improving the predictions.

Hutchinson and Whalley (1973) have assumed that the deposition rate is directly proportional to the droplets mass concentration C (kg/m^3) in the gas core:

$$\dot{m}_{\mathrm{D}} = kC, \tag{16}$$

where k is the mass transfer coefficient.

The entrainment rate is given by a relation identical to that of the deposition rate, but assuming that a hydrodynamic equilibrium is achieved:

$$\dot{m}_{\mathrm{E}} = kC_{\infty}, \tag{17}$$

where C_{∞} is the equilibrium droplet concentration. It remains to determine the expression of the equilibrium droplet concentration.

The model of Hutchinson and Whalley (1973) characterizes the entrainment mechanism, based on the shearing-off of roll wave crests, as the result of two opposing forces: the interfacial friction exerted at the interface film-gas, which tends to drag droplets from the film

surface and the surface tension stress, which keeps the liquid to the film surface. The ratio between the two forces is defined in terms of the following dimensionless group: $We_{GF} = \tau_{GF}\delta/\sigma$. We have expressed, analytically, the equilibrium droplet concentration by:

$$C_\infty = 124 We_{GF}^2. \tag{18}$$

As improvements to bring to the entrainment rate relation, Whalley and Hewitt (1978) had suggested to take into account the effect due to the formation of disturbance waves on the interface film-gas, which is directly dependent on the wave amplitude. According to Ishii and Mishima (1989), the wave amplitude is proportional to the film Reynolds number. This dimensionless number is precisely a varying parameter in the experiments of Cousins et al. (1965).

Consequently, we propose an adjustment from the experiences of Cousins *et al.*, assuming that the multiplier factor in (18) is no longer a constant, but a function of the film number Reynolds.

An iterative procedure is utilized to search for the numerical value of the multiplier factor which allows the predictions to approximate better than the experimental results, in different experimental conditions. A linear adjustment of the numerical results lead us to the following relation which is valid only for film Reynolds numbers of more than 800 (Ho-Kee-King, 1996):

$$C_\infty = 0.06[Re_F - Re_F^*]We_{GF}^2 \text{ with } Re_F^* = 800. \tag{19}$$

This limitation is similar to a condition of entrainment onset proposed by Dallman (1984), Andreussi (1983) or Schadel et al. (1990). It is one of the three main conditions of entrainment onset available in literature. The two other conditions are the minimum gas velocity defined by Ishii and Grolmes (1975), and the critical film Weber number We_{GF}^* according to Nigmatulin (1991). The former condition is always verified in the Cousins *et al.* experiences, and the last one is the only one which is not explicitly taken into account in the proposed entrainment rate relation (17) and (19). Then, we introduced it in the modified relation of Hutchinson and Whalley.

The entrainment rate is finally formulated as following:

$$\begin{cases} \dot{m}_E = kC_\infty;\ C_\infty = 0.06[Re_F - Re_F^*]We_{GF}^2 & \text{for } Re_F > Re_F^* = 800,\ We_{GF} > We_{GF}^* \\ \dot{m}_E = 0 & \text{for } Re_F \le Re_F^* = 800,\ We_{GF} \le We_{GF}^*. \end{cases} \tag{20}$$

Figure 8 illustrates the entrained fraction calculated from the preceding relation (Fig. 8, full line). The modification of Hutchinson's relation leads to obvious ameliorations for the two first experimental conditions with lower film Reynolds number. Prediction-data discrepancies still remain when Re_{LF} is equal to *932*, but the differences obtained earlier in Fig. 7 are now reduced by at least a factor of ten.

It is also noticed, in Fig. 8, that the entrainment rate is almost zero on a certain distance from the channel inlet, the length of the distance varies with the experimental conditions. This could correspond to the inlet region identified by Kataoka and Ishii (1983). The length suggested by these authors is given for a dimensionless distance ζ less than 160: this condition had been only verified for relatively high film Reynolds numbers. In the case of higher film

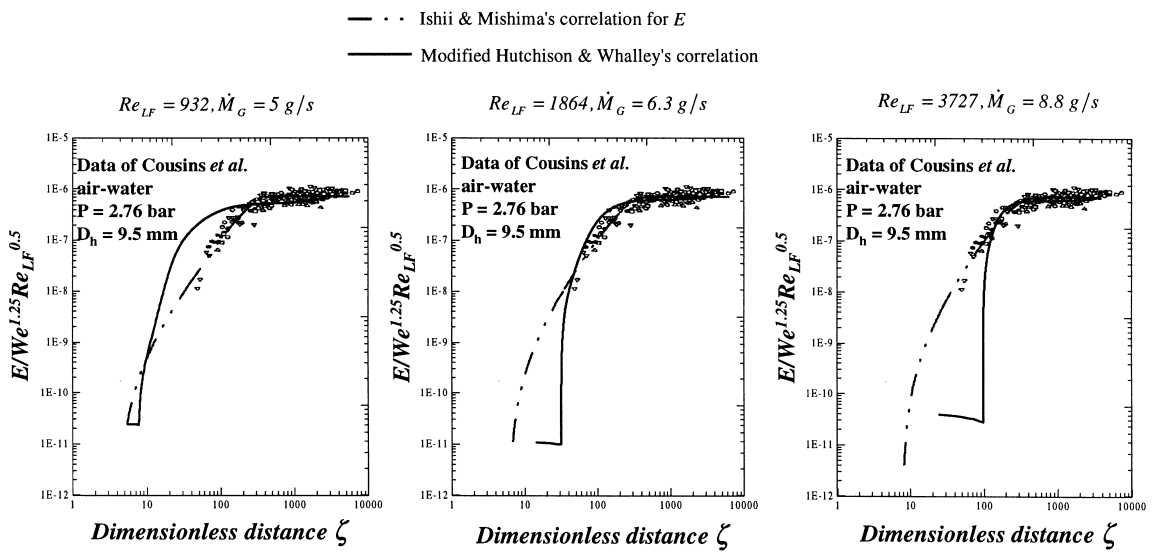

Fig. 8. Comparison of data of Cousins et al. (1965) with: (a) predicted entrained fraction from relation developed from Ishii and Mishima (1981); (b) predictions of three-field model obtained with the modification of the entrainment rate relation of Hutchinson and Whalley (1973).

Reynolds number ($Re_{LF} = 3727$, see Fig. 8), the entrainment rate is negligible for a dimensionless distance ζ less than 130: this is comparable with the condition suggested by Kataoka and Ishii (1983).

Although it still remains a discrepancy between predictions and data of the entrained fraction in the case of lower film Reynolds number, the entrainment rate correlation modified from Hutchinson's one, allows a rather good description of most of Cousins's experiences.

Consequently, we propose the following correlations as the deposition–entrainment model:

$$\begin{cases} \dot{m}_D = kC;\ k = 87u_*\sqrt{\dfrac{\mu_L^2}{D\sigma\rho_L}},\ u_* = \sqrt{\dfrac{\tau_{GF}}{\rho_G}} \\ \\ \dot{m}_E = kC_\infty;\ C_\infty = 0.06[Re_F - Re_F^*]We_{GF}^2 \quad \text{for } Re_F > Re_F^* = 800,\ We_{GF} > We_{GF}^*. \end{cases} \tag{21}$$

To resume the procedure followed progressively until here, our objective is to establish a three-field model which accounts for entrainment and deposition mechanisms in order to describe the experiments of Lemonnier and Selmer Olsen (1992) performed in a converging nozzle. As we have not found satisfying mass transfer relations, we are induced to modify the entrainment rate relation of Hutchinson et al. (1974) on the basis of experimental results of Cousins et al. (1965), who have measured the entrained liquid amount from the film surface to the flow core. A local entrainment rate relation, for a fixed deposition rate correlation, is established satisfactorily for the experiments of Cousins et al. (1965), we now revert to the experiences of Lemonnier and Selmer Olsen in a converging nozzle.

6. Predictions of the Three-field Model in a Converging Nozzle

To reach a good description of the experiments of Lemonnier and Selmer Olsen in a converging nozzle from the three-field model, in which entrainment and deposition rates had been correlated by (21), we have to modify some closure relations:

- on the one hand, the entrainment rate relation given by (20) will be completed with a condition on the film thickness, below which no further entrainment occurs in these experiences;
- and, on the other hand, the parietal film-wall friction relation of type Blasius will be modified to account for the effect of streaming gas flow.

For three different experimental conditions, presented in Fig. 9, with decreasing values of gas quality, the three-field model calculations showed, as those obtained with the original relation of Hutchinson et al. (1974), that:

- the liquid film is strongly broken away in the converging part of the nozzle, and the film thickness becomes very thin from the throat inlet: this is in conformity to Selmer Olsen's observations.
- and, in addition to the fact that the pressure drops too fast before the throat exit, the liquid break-away is going on inside the throat leading to a reduction of the film thickness, whereas Selmer Olsen measures a slight growth of the film thickness due to a liquid re-deposition.

So as to describe these experiments, the break-away in the nozzle throat must be limited. Any one of the existing conditions of entrainment onset have lead us to justify such a limitation (Ho-Kee-King, 1996).

Then, we suggest to take into account the existence of a singularity in the nozzle's profile, due to the presence of a junction between the converging and the throat by the consideration of the following mechanism:

- the break-away in the converging part of the nozzle is effective enough to generate a relatively "smooth" film flow, with low amplitude waves on the film surface;
- and the distance which is necessary for the growing wave to rise again to the shearing-off of the roll wave crest, is not achieved by the throat length.

The entrainment rate model in (20) is, therefore, completed, assuming that, in these experimental conditions, the film thickness is too thin to ensure the phenomena of shearing-off of roll wave crest. So, we add this condition:

$$\text{If } \delta < \delta^*, \delta^* = 100\ \mu\text{m}, \text{ then } \dot{m}_E = 0. \tag{22}$$

With the droplet entrainment rate correlated by (20) and (22), Fig. 10 shows that the film mass flowrate increases along the throat: that is the proof that the break-away is very limited for the three experimental conditions. Moreover, the trend in the evolution of the film thickness is well reproduced.

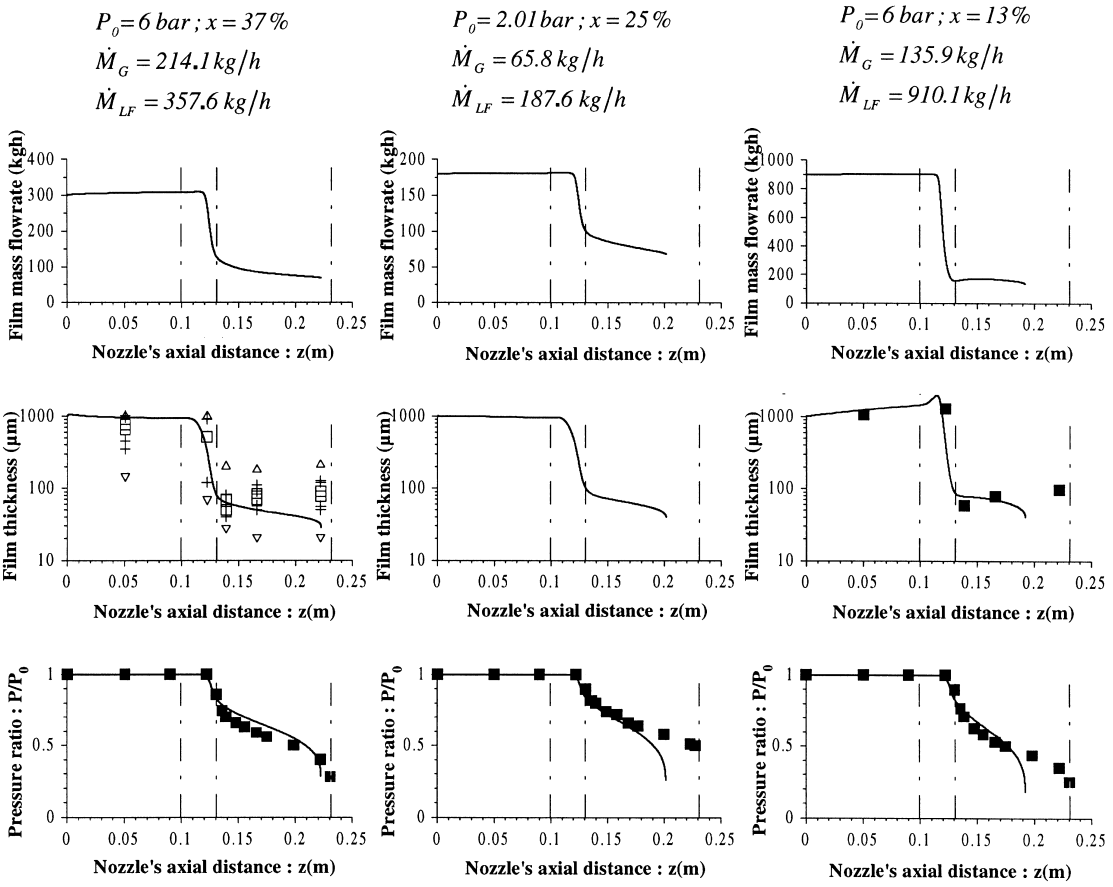

Fig. 9. Comparison of measured pressure and film thickness profiles (symbols) with predictions of the three-field model. The entrainment rate relation is modified from Hutchinson's one (20). The symbol (□) represents the mean film thicknesses, the crosses (+) indicate one standard deviation up or down and the arrow tips (△ and ▽) indicate extreme values.

Nevertheless, the pressure profiles show that:

- with a high gas quality, the predicted pressure profile is obviously beyond the experimental profile;
- with a low gas quality, the predicted pressure drop is too important in the throat; and
- for an intermediate value of the gas quality, the pressure profile is well predicted.

In order to locate the reasons, we have analyzed, from the total momentum balance, what terms have implied a strong pressure gradient.

The total momentum balance is expressed as follows:

$$-A\frac{\mathrm{d}P}{\mathrm{d}z} = \mathcal{P}_{\mathrm{Fp}}\tau_{\mathrm{Fp}} + \frac{\mathrm{d}(\dot{M}u)}{\mathrm{d}z}, \tag{23}$$

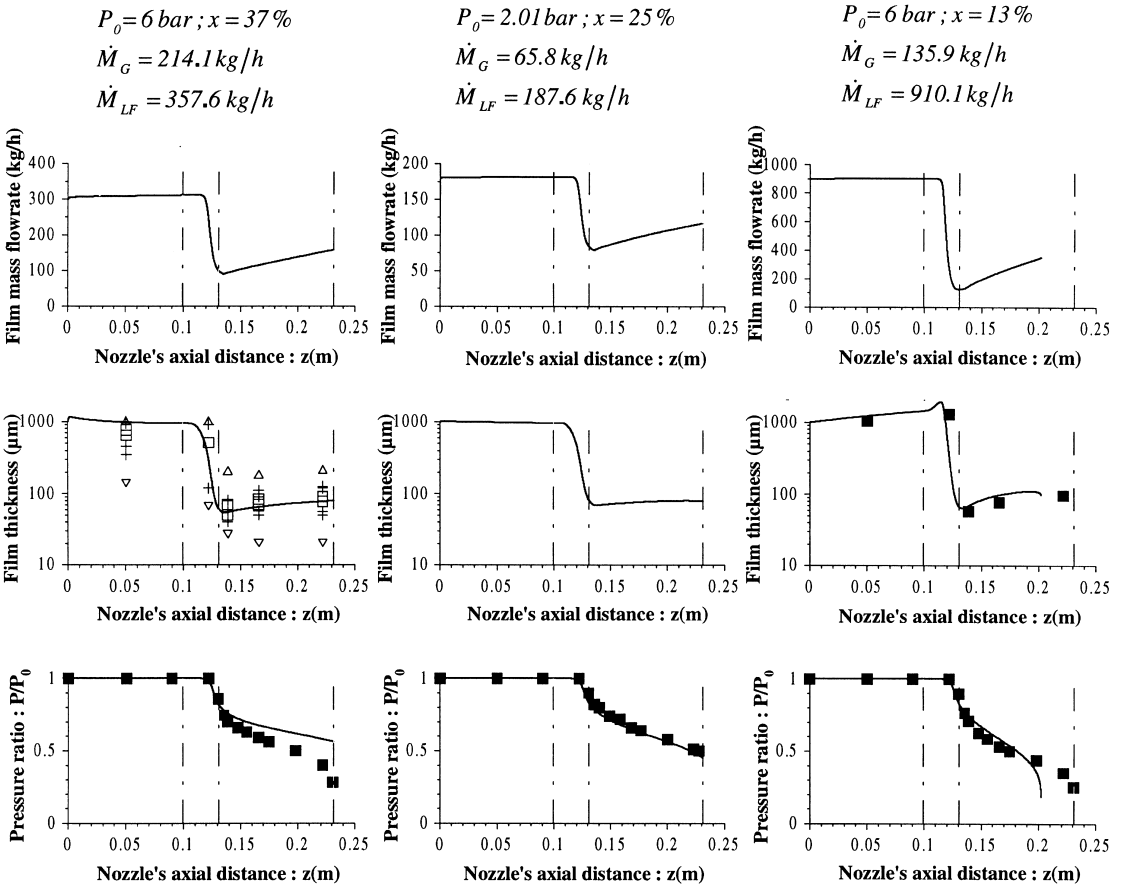

Fig. 10. Comparison of measured pressure and film thickness profiles (symbols) with predictions of the three-field model. The entrainment rate relation is given by (20) and (22). The symbol (□) represents the mean film thicknesses, the crosses (+) indicate one standard deviation up or down and the arrow tips (△ and ▽) indicate extreme values.

where $\mathcal{P}_{\mathrm{Fp}}$ is the pipe perimeter, $\mathrm{d}P/\mathrm{d}z$ the total pressure gradient, and the rate of change of the total momentum is given by:

$$\frac{\mathrm{d}(\dot{M}u)}{\mathrm{d}z} \equiv \sum_{k=\mathrm{G,F,L}} \frac{\mathrm{d}(\dot{M}_k u_k)}{\mathrm{d}z}. \tag{24}$$

In (23), the two main constituents of total pressure gradient are the parietal friction exerted from the film, and the rate of change of total flow momentum.

This last term is preponderant in the converging part, with an order of magnitude relatively important, and it has the same order of magnitude with the friction stress in the throat (Fig. 11). A priori, the term which has a significant influence on the pressure drop, only in the nozzle throat, is the parietal friction. Consequently, we have modified the parietal friction relation in order to introduce the influence of gas quality.

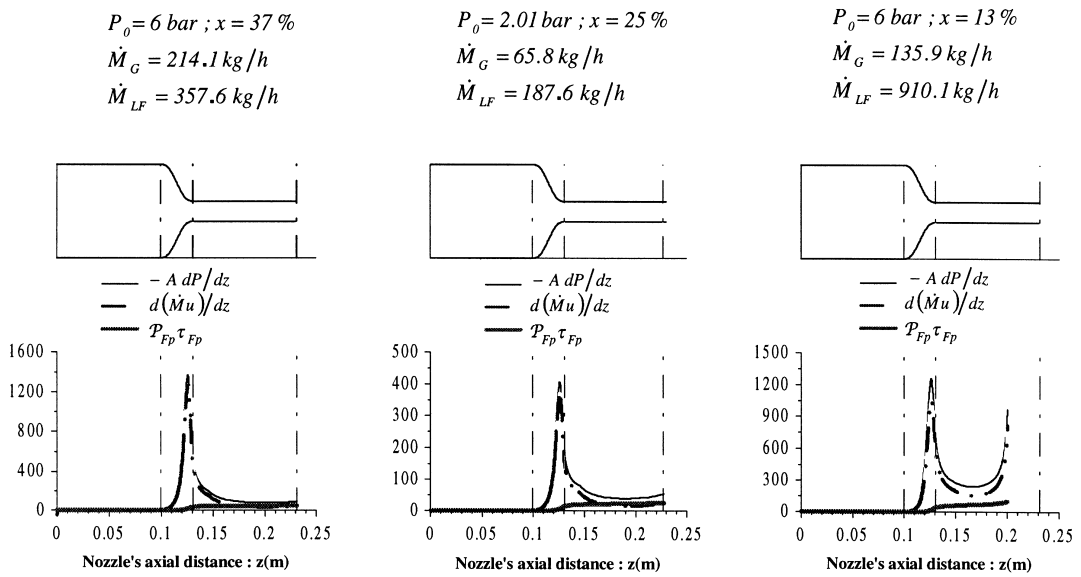

Fig. 11. Order of magnitude of the various terms which appear explicitly in the total momentum balance equation (23).

For the considered experimental conditions, the film flow is turbulent and the parietal friction is correlated by (8) (Nigmatulin, 1991). We assume that, as the film thickness is very thin from the throat, the parietal friction is intensified by the streaming gas flow when the gas quality is relatively high.

With an adjustment from experimental conditions, the parietal friction coefficient is so correlated (Ho-Kee-King, 1996):

$$\tau_{\mathrm{Fp}} = \frac{1}{2} C_{\mathrm{w}} \rho_{\mathrm{F}} u_{\mathrm{F}}^2;\ C_{\mathrm{w}} = 0.0791 Re_{\mathrm{F}}^{-0.25}[1 + (24.5x^2 - 6.45x)]. \tag{25}$$

We have imposed for the adjustment that the parietal friction coefficient tends to Blasius's one for a liquid single phase flow when the gas quality tends towards 0.

With such a modification, the three-field model predicts, at best, the data of pressure and film thickness along the converging nozzle (Fig. 12). A slight insufficiency in predicted pressure drop, in the case of lower gas quality, is noticed.

The three-field model finally proposed here is validated successfully with three different experimental conditions. Now, we will apply it to the whole of Lemonnier's experiments performed at an upstream pressure of 2 bar, varying total liquid mass flowrates.

In these experiments, the three-field model has been completed for the cases of low liquid mass flowrates. It has already been mentioned that in such conditions the two-phase flow is essentially dispersed and the two-field model gives good predictions for maximum gas mass flowrates and exit droplet velocities.

When the liquid flowrate is low (less than 50 kg/h), the predicted film thickness is too thin (about 10 μm). Furthermore, the film flow is laminar, so the interfacial friction exerted between

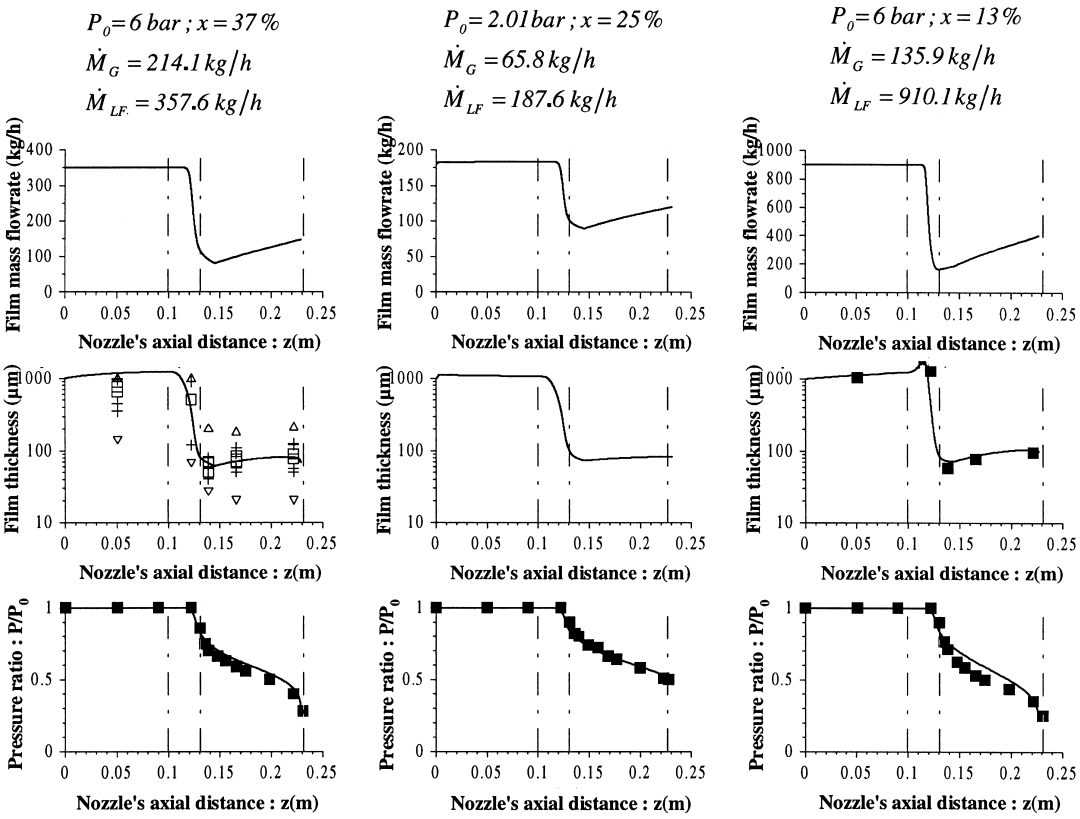

Fig. 12. Comparison of measured pressure and film thickness profiles (symbols) with predictions of the three-field model. The parietal friction coefficient is modified with a multiplier factor function of gas quality x (25). The symbol (□) represents the mean film thicknesses, the crosses (+) indicate one standard deviation up or down, and the arrow tips (△ and ▽) indicate extreme values.

the film surface and the gas core is very high, increasing in this way the film velocity. In these conditions, with a very thin film thickness and a high film velocity, the singularity in the nozzle shape due to the junction between the convergent and the throat, which has already been underlined previously, leads now to a quasi-total atomization of the film to the gas core from the throat inlet (Ho-Kee-King, 1996).

Predictions of the three-field model that we finally proposed in this paper reproduce rather well all the data for maximum gas mass flowrates and exit droplet velocities, at an upstream pressure of 2 bar (Fig. 13).

7. Conclusions

We have shown that air–water flows of which the configuration is annular dispersed, can be predicted well only with a three-field model, accounting for entrainment and deposition mechanisms. It has also been observed (Boyer and Lemonnier 1996) that for steam–water flows in a Venturi tube, the pressure drop was better predicted with a three-field model.

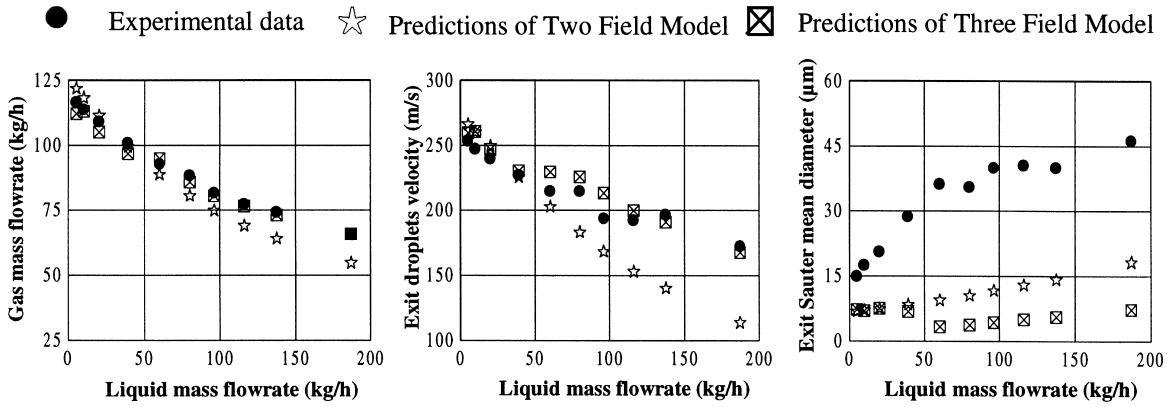

Fig. 13. Comparison of experimental data (circular symbols) with: (a) predictions of the three-field model (checked-square symbols); (b) predictions of the two-field model (star symbols), for an upstream pressure constant equal to 2 bar, and varying total liquid mass flow-rates.

The objective of this paper is to reach a good description of the experiments of Lemonnier and Camelo (1993) and Selmer Olsen (1991), performed in a converging nozzle with an annular liquid injection. In the case of such liquid injection mode, Selmer Olsen (1991) has observed that the liquid film is violently atomized at the throat inlet. This behavior is well reproduced with the three-field model proposed here, and in which we had had to take into account the multidimensional effects due to the change of cross-sectional area in the nozzle: depending on whether the liquid mass flowrate is important or not, the liquid film is partially or totally atomized from the throat inlet.

Accounting for the effect of the singularity due to the junction convergent-throat, can justify a multidimensional modeling.

With the three-field model, it has been possible to describe successfully most of the available experimental data: pressure profiles, maximum gas mass flowrate, exit droplet velocities, and film thicknesses.

However, some differences between predictions and the data still remain unexplained:

- The predicted droplet size is always underestimated. This disagreement is probably not only due to the drop size correlation. It is conceivable that a phenomenon of coagulation at the nozzle exit occurs on droplets of small size and of velocity close to the gas velocity.
- The pressure drop is sometimes slightly insufficient inside the throat. This has been more recently highlighted (Lemonnier H., CEA/Grenoble): a detachment of the film flowing on the walls should occur at the vicinity of the throat inlet.

The instantaneous nature of some processes will probably be to question. Not only as suggested by Selmer Olsen for the drop size correlation, where it will be necessary to consider a process of break-up combined with a certain relaxation time, but also for the entrainment and deposition phenomena: a certain transit time is necessary to allow the droplets broken away from the film surface, thus of velocity close to film velocity, to reach the velocity of droplets flowing in the gas core flow, which is close to the gas velocity.

Improvements are planned, with the contribution of data of entrained liquid fraction and liquid film thickness recently collected by Camelo et al. (1995). All these data will serve as a basis for a further refining of the three-field model, incorporating the mechanisms invoked form our analysis. These mechanisms have also been invoked from some authors (Hutchinson et al., 1974; Azzopardi et al., 1991; Azzopardi, 1992, 1993; Hills, 1997), and their works will constitute a reference for our investigations.

Appendix A

A.1. Two-field model : totally dispersed two-phase flow model.

Fig. A1

$$\frac{\mathrm{d}}{\mathrm{d}z}[\dot{M}_{\mathrm{G}}] = 0,$$

$$\frac{\mathrm{d}}{\mathrm{d}z}[\dot{M}_{\mathrm{L}}] = 0,$$

$$\frac{\mathrm{d}}{\mathrm{d}z}[\dot{M}_{\mathrm{G}} u_{\mathrm{G}}] + A_{\mathrm{G}} \frac{\mathrm{d}P}{\mathrm{d}z} = -\mathcal{P}\tau_{\mathrm{Gp}} - \mathcal{P}_{\mathrm{LG}}\tau_{\mathrm{GL}},$$

$$\frac{\mathrm{d}}{\mathrm{d}z}[\dot{M}_{\mathrm{L}} u_{\mathrm{L}}] + A_{\mathrm{L}} \frac{\mathrm{d}P}{\mathrm{d}z} = \mathcal{P}_{\mathrm{LG}}\tau_{\mathrm{GL}},$$

$$\frac{\mathrm{d}}{\mathrm{d}z}\left[\dot{M}_{\mathrm{G}}\left(H_{\mathrm{G}} + \frac{1}{2}u_{\mathrm{G}}^2\right)\right] = \mathcal{P}_{\mathrm{LG}}\tau_{\mathrm{GL}}u_{\mathrm{L}} - \mathcal{P}_{\mathrm{LG}}\dot{Q}_{\mathrm{LG}},$$

$$\frac{\mathrm{d}}{\mathrm{d}z}\left[\dot{M}_{\mathrm{L}}\left(H_{\mathrm{L}} + \frac{1}{2}u_{\mathrm{L}}^2\right)\right] = \mathcal{P}_{\mathrm{LG}}\tau_{\mathrm{GL}}u_{\mathrm{L}} - \mathcal{P}_{\mathrm{LG}}\dot{Q}_{\mathrm{LG}},$$

$$\frac{\mathrm{d}}{\mathrm{d}z}[A_{\mathrm{G}} + A_{\mathrm{L}}] = \frac{\mathrm{d}A}{\mathrm{d}z},$$

where the subscripts "G" and "L" refer to the gas and the liquid droplet phase, respectively, $\dot{M}$ the mass flowrate (kg/s), u the area-averaged velocity (m/s), H the area-averaged mass enthalpy (J/kg), P the area-averaged mixture pressure (N/m^2), A_G the cross-sectional area occupied from the gas phase (m^2), A_L the cross-sectional area occupied from the dispersed liquid phase (m^2), A the pipe cross-sectional area (m^2), $\mathcal{P}$ the pipe perimeter (m), $\mathcal{P}_{LG}$ the perimeter between the gas and the liquid droplets (m), τ the friction stress (N/m^2), and $\dot{Q}$ the heat flux (J/s.m^2).

The independent variables are the following: $\dot{M}_G$, $\dot{M}_L$, u_G, u_L, H_G, H_L and P.

A.2. PAFM: purely annular two-phase flow model.

Fig. A2

$$\frac{d}{dz}[\dot{M}_G] = 0,$$

$$\frac{d}{dz}[\dot{M}_F] = 0,$$

$$\frac{d}{dz}[\dot{M}_G u_G] + A_G \frac{dP}{dz} = -\mathcal{P}_{FG}\tau_{GF},$$

$$\frac{d}{dz}[\dot{M}_F u_F] + A_F \frac{dP}{dz} = -\mathcal{P}\tau_{Fp} + \mathcal{P}_{FG}\tau_{GF},$$

$$\frac{d}{dz}\left[\dot{M}_G\left(H_G + \frac{1}{2}u_G^2\right)\right] = -\mathcal{P}_{FG}\tau_{GF}u_{FG} + \mathcal{P}_{FG}\dot{Q}_{FG},$$

$$\frac{d}{dz}\left[\dot{M}_F\left(H_F + \frac{1}{2}u_F^2\right)\right] = \mathcal{P}_{FG}\tau_{GF}u_{FG} - \mathcal{P}_{FG}\dot{Q}_{FG},$$

$$\frac{d}{dz}[A_G + A_F] = \frac{dA}{dz},$$

where the subscripts "G" and "F" refer to the gas and the liquid film phase, respectively, A_F the cross-sectional area occupied from the liquid film phase (m^2), and $\mathcal{P}_{FG}$ the perimeter between the gas and the liquid film surface (m).

The independent variables are the following: $\dot{M}_G$, $\dot{M}_F$, u_G, u_F, H_G, H_F and P.

A.3. Three-field model : annular dispersed two-phase flow model.

Fig. A3

$$\frac{d}{dz}[\dot{M}_G] = 0,$$

$$\frac{d}{dz}[\dot{M}_F] = \mathcal{P}_{FG}(\dot{m}_D - \dot{m}_E),$$

$$\frac{d}{dz}[\dot{M}_L] = -\mathcal{P}_{FG}(\dot{m}_D - \dot{m}_E),$$

$$\frac{d}{dz}[\dot{M}_G u_G] + A_G \frac{dP}{dz} = -\mathcal{P}_{FG}\tau_{GF} - \mathcal{P}_{LG}\tau_{GL},$$

$$\frac{d}{dz}[\dot{M}_F u_F] + A_F \frac{dP}{dz} = -\mathcal{P}_{pF}\tau_{Fp} + \mathcal{P}_{FG}\tau_{GF} + \mathcal{P}_{FG}\dot{m}_D u_L - \mathcal{P}_{FG}\dot{m}_E u_{FG},$$

$$\frac{d}{dz}[\dot{M}_L u_L] + A_L \frac{dP}{dz} = \mathcal{P}_{LG}\tau_{GL} - \mathcal{P}_{FG}\dot{m}_D u_L + \mathcal{P}_{FG}\dot{m}_E u_{FG},$$

$$\frac{d}{dz}\left[\dot{M}_G\left(H_G + \frac{1}{2}u_G^2\right)\right] = -\mathcal{P}_{FG}\tau_{GF}u_{FG} - \mathcal{P}_{LG}\tau_{GL}u_L + \mathcal{P}_{LG}\dot{Q}_{LG} + \mathcal{P}_{FG}\dot{Q}_{FG},$$

$$\frac{d}{dz}\left[\dot{M}_F\left(H_F + \frac{1}{2}u_F^2\right)\right] = \mathcal{P}_{FG}\tau_{GF}u_{FG} - \mathcal{P}_{FG}\dot{Q}_{FG} + \mathcal{P}_{FG}\dot{m}_D\left(H_L + \frac{1}{2}u_L^2\right) - \mathcal{P}_{FG}\dot{m}_E\left(H_F + \frac{1}{2}u_{FG}^2\right),$$

$$\frac{d}{dz}\left[\dot{M}_L\left(H_L + \frac{1}{2}u_L^2\right)\right] = \mathcal{P}_{LG}\tau_{GL}u_L - \mathcal{P}_{LG}\dot{Q}_{LG} - \mathcal{P}_{LG}\dot{m}_D\left(H_L + \frac{1}{2}u_L^2\right) + \mathcal{P}_{FG}\dot{m}_E\left(H_F + \frac{1}{2}u_{FG}^2\right),$$

$$\frac{d}{dz}[A_G + A_F + A_L] = \frac{dA}{dz}.$$

The independent variables are the following: $\dot{M}_G$, $\dot{M}_F$, $\dot{M}_F$, u_G, u_F, u_L, H_G, H_F, H_L and P.

References

Andreussi, P., 1983. Droplet transfer in two-phase annular flow. Int. J. Multiphase flow 9 (6), 697–713.

Azzopardi, B.J., Texeira, S.F.C.F., Govan, A.H., Bott, T.R., 1991. An improved model for pressure drop in venturi scrubbers. Trans. IChemE, B 9, 237–245.

Azzopardi, B.J., 1992. Gas-liquid flows in cylindrical venturi scrubbers: boundary layer separation in the diffuser section. Chem. Engng Sci. 49, 55–64.

Azzopardi, B.J., 1993. Liquid distribution in venturi scrubbers: boundary layer separation in the diffuser section. Chem. Engng Sci. 48, 2807–2813.

Berne, Ph, 1983. Contribution à la mod élisation du taux de production de vapeur par autovaporisation dans les écoulements diphasiques en conduite. Thèse de Docteur Ingénieur, Ecole Centrale des Arts et Manufactures, Paris, France.

Bilicky, Z., Dafermes, C., Kestin, J., Majda, G., Zeng, D.L., 1987. Trajectories and singular points in steady-state models of two-phase flows. Int. J. Multiphase Flow 13 (4), 511–533.

Bird, R.B., Stewart, W.E., Lightfoot, E.N., 1960. Transport Phenomena. Wiley, New York.

Boyer, C., Lemonnier, H., 1996. Design of a flow metering process for two-phase dispersed flows. Int. J. Multiphase Flow 22 (4), 713–732.

Camelo, E., Lemonnier, H., Ochterbeck, J., Selmer, Olsen S., 1995. Characterization of non equilibrium effects on high quality critical flows. Nureth 7 Proc, Saratoga Springs, New York, Sept. 10–15, Rapport NUREG/CP-0142 vol. 1, 111–130.

Cousins, L.B., Denton, W.H., Hewitt, G.F., 1965. Liquid mass transfer in annular two-phase flow. Symp. on Two-Phase Flow, Exeter, UK vol. 1, Paper C4.

Dallman, J.C., Laurinat, J.E., Hanratty, T.J., 1984. Entrainment for horizontal annular gas–liquid flow. Int. J. Multiphase Flow 10 (6), 677–690.

Dobran, F., 1987. Nonequilibrium modeling of two-phase critical flows in tubes. J. Heat Transfer 109, 731–738.

Hewitt, G.F., Govan, H., 1990. Phenomenological modelling of non-equilibrium flows with phase change. Int. J. Heat Mass Transfer 33 (2), 229–242.

Hills, J.H. 1997. The critical flowrates for wave and droplet formation in annular gas–liquid flow. In: Giot, M., Mayinger, F., Celata, GP. (Eds.), Experimental Heat Transfer, Fluid Mechanics and Thermodynamics. Edizione ETS, Italy. vol. 2. pp. 1241–1247.

Hutchinson, P., Whalley, P.B., 1973. A possible characterization of entrainment in annular flow. Chem. Engng. Sci. 28, 974–975.

Hutchinson, P., Whalley, P.B., Hewitt, G.F., 1974. Transient flow redistribution in annular two-phase flow. Int. J. Multiphase Flow 1, 383–393.

Ho-Kee-King, S., 1996. Contribution à la modélisation des écoulements diphasiques en canalisation: influence des processus d'entraînement et de déposition dans le cas d'une configuration annulaire dispersée. Thèse de Doctorat de l'Université Paris XII-Val de Marne, France.

Ishii, M., Grolmes, M.A., 1975. Inception criteria for droplet entrainment in two-phase concurrent film flow. AIChE J. 21 (2), 308–318.

Ishii, M., Mishima, K., 1981. Correlation for liquid entrainment in annular two-phase flow of low viscous fluid. Argonne Laboratory Report, ANL/RAS/LWR 81-2.

Ishii, M., Mishima, K., 1989. Droplet entrainment correlation in annular two-phase flow. Int. J. Heat Mass Transfer 32 (10), 1835–1846.

Kataoka, I., Ishii, M. 1983. Entrainment and deposition rates of droplets in annular two-phase flow. In: Mori, Y., Yang, W.J. (Eds.), Proc. ASME-JSME Thermal Engng Joint Conference. ASME, New York, vol. 1. pp. 69–80.

Lemonnier, H., Selmer, Olsen S., 1992. Experimental investigation and physical modelling of two-phase two-component flow in a converging-diverging nozzle. Int. J. Multiphase Flow 18 (1), 1–20.

Lemonnier, H., Camelo, Cavalcanti E.S., 1993. Droplet size and velocity at the exit of a nozzle with two-component near-critical and critical flow. ANS Proceedings, 1993 National Heat Transfer Conference, American Nuclear Society vol. 7, 93–100.

Nigmatulin, R.I., Nigmatulin, B.I., Khodzhaev, Y.A., Kroshilin, V.E., 1996. Entrainment and deposition rates in a dispersed-film flow. Int. J. Multiphase Flow 22 (1), 19–30.

Nigmatulin, R.I., 1991. Dynamics of multiphase media, vol. 2. Section 7, Hemisphere.

Paleev, I.I., Filippovich, B.S., 1966. Phenomena of liquid transfer in two-phase dispersed annular flow. Int. J. Heat Mass Transfer 9, 1089–1093.

Richter, H.J., 1983. Separated two-phase flow model: application to critical two-phase flow. Int. J. Multiphase Flow 9 (5), 511–530.

Selmer, Olsen S., 1991. Etude théorique et expérimentale des écoulements diphasiques en tuyère convergente-divergente. Thèse de Doctorat de l'Institut National Polytechnique de Grenoble, France.

Schadel, S.A., Leman, G.W., Binder, J.L., Hanratty, T.J., 1990. Rates of atomization and deposition in vertical annular flow. Int. J. Multiphase Flow 16 (3), 363–374.

Whalley, P.B., Hewitt, G.F., 1978. The correlation of liquid entrainment fraction and entrainment rate in annular two-phase flow, Rept. AERE-R9187. UKAEA, Harwell.